Influence of annealing temperature on the properties of ZnO nanostructures

Mohammad M. Ali*, Saeed J. Abbas and Alaa S. Al-Kabbi

Department of Physics, College of Science, University of Basrah, Basrah, Iraq

**E-mail: moh7077ali@gmail.com*

Doi 10.29072/basjs.201902014

Abstract

The effects of annealing process on the properties of ZnO nanostructures was investigated using XRD, SEM and UV-visible spectrometry techniques in the range of 300-450°C. XRD measurements showed that the deposited and annealed ZnO nanostructures have hexagonal (wurtzite) structure without external impurities. (002) plane is the preferred orientation for ZnO nanostructures thin films. Lattice parameters, crystalline size, bond length between Zn and O (Zn-O), etc. were determined for ZnO nanostructures thin films. The lattice constants a=b= 3.278 Å, c= 5.251 Å for as-deposited and gradually decreased to a=b= 3.259 Å, c= 5.220 Å after the annealing at a temperature 450°C. The increase in annealing temperature (Ta) lead to increase in the intensity of the diffraction peaks. As the temperature of annealing increases, particle size increases and nano-needles (NNs) rise and become more oriented. Williamson-Hall (W-H) analysis was used to evaluate crystallite sizes and lattice strain based on X-ray peak broadening analysis. The results showed that there is a very large inter-correlation between the estimated crystallite size from Scherer's formula and W-H plots. The films are found optically transparent for visible region of the electromagnetic spectrum with the average value of transmittance (90% to 95%) and it seems depending on the Ta. There is somewhat agreement between the estimated band gap value from optical measurements with the band gap value for bulk ZnO (for as-deposited films of ZnO nanostructures). The band gap decreases with Ta (Eg = 3.26 eV of as-deposited films and after annealing, it decreases to 3.20 eV, 3.17 eV, 3.10 eV and 3.06 eV, respectively).

Keywords: Annealing effect; X-ray analysis; ZnO nanostructures; branching structures; optical properties

1. Introduction

There is great interest in transparent conductive oxide (TCO) films where they play an important role in many devices such as flat panel displays, light-emitting diodes and solar cells [1]. Indium tin oxide (ITO) is the most important of these transparent films, having a low

resistivity of 10^{-4} Ω.cm and transmittance (> 85%) for visible rays [2]. However, ITO instability as well as the scarcity and toxicity of indium have reduced its use and the search for alternative TCO materials [3,4]. Zinc oxide (ZnO) is a semiconductor material with multiple uses in sensors, optoelectronics and catalysis [5]. Thin films of ZnO with high electrical conductivity, high transmittance for visible rays and infrared reflection can be obtained through various coating techniques [6]. ZnO has a direct band gap (3.37 eV) and binding energy of the exciton of ZnO (60 meV) and is therefore used for excitonic devices [7], this large energy can lead to lasing action even above room temperature based on the recombination of the exciton. ZnO supplied a large variety of one-dimensional (1D) nanostructures such as nano-tubes, nano-wires, nano-rods and nano-needles [8-11]. Reducing the size of materials to the nanometer range (such as 1D nanostructures) lead to appearance of quantization effects due to the confinement of the movement of electrons, making the properties of the material such as electrical and thermal transport depends on the dimensions and size reduction [12].

ZnO nanostructures have different properties than bulk ZnO, so it has been successfully prepared using many techniques. Among these techniques are mentioned in works [13-17] as well as Thermal Evaporation (T.E). T.E is one of the most suitable techniques to deposit films, environmentally friendly, with the possibility of controlling growth factors such as deposition rate and film thickness [18]. ZnO thin films can be grown on different substrates but the glass substrate is suitable due to its cheap and availability.

In this work, the nanostructures of ZnO thin films were prepared by T.E technique and the effect of Ta on the structural, morphology, composition and optical properties was studied.

2. Experimental

The glass substrates (Microscope slides, CAT.No.7101) were cleaned in several detergents for 10 minutes in each case using an ultrasonic bath such as acetone, ethanol and DI water. It was then exposed to the pure N_2 gas for drying and dust removal. The cleaned substrates were installed in the vacuum chamber and kept at room temperature (RT) during the coating process. Zinc powder has purity around 99.999% was loaded in the tungsten boat and placed in the vacuum chamber. The distance between the zinc source and the substrates were 10 cm. The pressure of 10^{-3}- 10^{-4} Torr was achieved in the vacuum chamber and maintained during the coating. Firstly, source materials are evaporated by the heated source. The evaporated material was then deposit onto the glass substrate. The weight difference method was used to measure the thickness of the ZnO thin film by using 6 digits sensitive microbalance. The thin

films of ZnO then undergo annealing process with a temperature ranges from 300-450°C for one hour, then the samples are allowed to cool down to RT. The structure of ZnO nanostructures was determined by using XRD (X'pert pro PANalytical company) with CuKα radiation of 1.5406 Å wavelength in the range from 20° to 70°. ZEISS SUPRA 55 VP (SEM) was used to study the morphology of the particles. The chemical composition of samples was studied using the dispersive X-ray spectrometer BRUKER X-Flash 6160 (EDS) associated with SEM. The Helios α UV-vis spectrophotometer (Thermospectronic, England) was used to study optical properties at wavelengths ranging from 300-1100 nm.

3. Results and discussion

3.1. Structural studies

The XRD patterns of the as-deposited and annealed ZnO nanostructures at 300°C, 350°C, 400°C and 450°C with prominent reflection planes is shown in Fig. 1. All the XRD peaks were indexed by hexagonal wurtzite phase of ZnO (JCPDS Card No. 36-1415). Diffraction peaks are observed at 31.4817^{o}, 34.1221^{o}, 35.9481^{o}, 47.3054^{o}, 56.3098^{o}, 62.6567^{o}, 67.8668 and 69.0077^{o} in the as-deposited film, which can be indexed as diffractions of (100), (002), (101), (102), (110), (103), (112) and (201) planes of hexagonal wurtzite structured ZnO. A clear peak broadening in the XRD pattern indicates to the presence of small nanocrystals in the samples. The peaks belonging to (100), (002) and (101) planes are clearly observed in all the ZnO nanostructures thin films which have highly intensity than other peaks. The prominent peak (002) in the XRD pattern indicates the preferential orientation of the c-axis of the crystals [19]. It can be observed that the structure became more ordered by gradually increasing the intensity of all peaks as the Ta increases. The lattice parameters of the wurtzite structure of the as-deposited and annealed ZnO nanostructures thin films can be calculated according to the following equation [20]:

$$\frac{1}{d^2_{(hkl)}} = \frac{4}{3}\left(\frac{h^2 + hk + k^2}{a^2}\right) + \frac{l^2}{c^2} \quad (1)$$

Where d is the spacing between the planes in the atomic lattice, (hkl) are Miller indices and a and c are the lattice constants.

According to Bragg's law [20]:

$$n\lambda = 2d \sin\theta \quad (2)$$

Where n is the order of diffraction (usually n=1) and λ is the X-ray wavelength.

With the first-order approximation, n=1:

$$\sin^2\theta = \frac{\lambda^2}{4a^2}\left[\frac{4}{3}(h^2 + hk + k^2) + \left(\frac{a}{c}\right)^2 l^2\right] \quad (3)$$

For plane (100), the lattice constant a is determined by the relationship [20]:

$$a = \frac{\lambda}{\sqrt{3}\sin\theta} \tag{4}$$

And for plane (002), the lattice constant c is determined by the relationship [20]:

$$c = \frac{\lambda}{\sin\theta} \tag{5}$$

The lattice constants calculated from XRD data (a=b=3.278Å and c=5.251Å with c/a=1.601) agree with the JCPDS standard data (Card No 36-1451).
The unit cell volumes are calculated by:

$$V = \frac{\sqrt{3}a^2c}{2} = 0.866\, a^2 \tag{6}$$

ZnO nanostructures can contain a number of defects that may affect their properties such as lattice disorders, oxygen vacancies, etc. To remove these defects is done by thermal annealing which results in lattice contracts. The dangling bonds on the surface of the ZnO cause the lattice relaxation. These bonds interact with oxygen ions in the atmosphere and due to electrostatic attraction, forming a slightly contracted lattice [21,22]. This can be seen from the decrease in lattice constants and the unit cell volumes with increasing Ta. Table 1 shows the variation of the lattice constants a and c with Ta and (dhkl) calculated from XRD and compared with the JCPDS standard data card and corresponding (hkl) planes.

The strong and sharp diffraction peaks can showed with increase Ta which indicate the formation of well crystallized sample. Figure 2 shows the effect of Ta on intensity, it indicates that as Ta increasing the intensity becomes higher with the increased narrowing of the diffraction peaks, which suggests that nanostructures become more crystalline, as well as increasing the sizes of crystallite.

3.2. Crystallite size and strain

3.2.1. Scherrer method

The Scherrer formula was used to calculate the average particle size (D) of the as-deposited and annealed ZnO nanostructures thin films, based on the full width half maxima of the XRD (100), (002) and (101) peaks of each sample [20].

$$D = \frac{k\lambda}{\beta\cos\theta} \tag{7}$$

Where k is a constant (shape factor = 0.90), λ is the wavelength of the X-rays (0.15406 nm), β is the FWHM in radians and θ is the angle of diffraction. Table 2 gives the crystallite size

of the as-deposited and annealed ZnO nanostructures thin films along prominent diffraction planes. An increase in Ta increases the sizes of the crystallite as shown in Fig. 3, which indicates that temperature plays an important role in tuning the sizes of the material crystals. In most cases the particle size is not the same as the size of the crystallite as the size of the crystallite represents the size of a coherently diffraction domain.

The length of the dislocation lines per unit crystal volume represents the amount of defects in the sample, known as the dislocation density (δ), and is calculated using equation (8) [23]:

$$\delta = \frac{1}{D^2} \tag{8}$$

The length of the bond L between oxygen and zinc atoms can be calculated using the relation [24]:

$$L = \sqrt{\left(\frac{a^2}{3} + \left(\frac{1}{2} - u\right)^2 c^2\right)} \tag{9}$$

Where u is a measure of the displacement amount of each atom relative to the next atom along the c-axis, which means positional parameter, and u can be given by the following relation [24]:

$$u = \frac{a^2}{3c^2} + 0.25 \tag{10}$$

The values obtained for the bond length are indicated in Table 2. The bond length of Zn-O is 2.21 Å, as the ionic radius of Zn is 0.83 Å [25] and O_2 is 1.83 Å [26].

From the relation (10), we notice that if the ratio of c/a is decreased, u increases, so that the four tetrahedral distances are constant by distorting the tetrahedral angles, indicating that u is inversely related with the ratio c/a [27].

Note from Table 2 that the change in the size of the crystallize is associated with the change in Ta, i.e. there is a decrease in the unit cell volume with the increase of Ta. The reason for the change in crystallize size may be due to the fact that ZnO nanoparticles include a large number of vacant clusters, oxygen vacancies, and interface disorders (local lattice disorders). The interface structure may be relaxed at low Ta, but it does not make apparent changes in the positions and intensities of XRD peaks, due to its inability to change the internal structure of nanograins or dissipate local lattice disorders. When Ta increases, the density of vacant lattice sites decreases rapidly, so are vacancy clusters and local lattice disorders, and rapid changes in the lattice parameters and unit cell volume occur, leading to grain growth, with increasing particle size [28]. The surface layer of ZnO nanoparticles has dangling bonds that cause the lattice to contraction. These dangling bonds, represented by ions, are incompletely coordinated and have unpaired electron orbitals. The dangling bonds are the Zn^{2+} and O^{2-} ions that form an array of parallel dipoles in the boundary layer of nanoparticles that exhibit repulsive force. Adsorption of O^{2-} and O^{-} ions occurs in the surface of ZnO, which leads to decreased of

repulsion interdipolar force and increased attractive electrostatic interaction between Zn^{2+} and O^{2-} ions which results in slightly contracted in lattice.

3.2.2. Williamson-Hall (W-H) methods

XRD profiles are not only influenced by the size of the crystallite, but may also by lattice defects and lattice strain. W-H method relies on the principle that the approximate formula for size broadening (β_D) and strain broadening (β_ε), vary quite differently with respect to Bragg angle θ [29]. The size broadening can be described in the Debye-Scherer (β_D) formula given in equation (7). The strain in thin film is defined as the disarrangement of lattice created during their deposition and depends upon the deposition parameters. The strain (ε) is obtained by using the equation (11):

$$\beta_\varepsilon = 4\varepsilon \tan\theta \tag{11}$$

The ε can be calculated from the observed broadening represented by either the maximum tensile strain alone or the maximum compressive strain alone. One symbolizes (β_D) and contribution varies as 1/cosθ and the other symbolizes (β_ε) and varies as tanθ. If both crystallite size and strain contributions present independently to each other, then their combined effects can be determined by convolution. The simplification of W-H is to assume the convolution is sum of β_D and β_ε.

$$\beta_{hkl} = \beta_D + \beta_\varepsilon \tag{12}$$

$$\beta_{hkl} = \frac{k\lambda}{D\cos\theta} + 4\varepsilon\tan\theta \tag{13}$$

$$\beta_{hkl}\cos\theta = \left(\frac{k\lambda}{D}\right) + (4\varepsilon\sin\theta) \tag{14}$$

Equation (14) means the Uniform Deformation Model (UDM) where strain is assumed to be uniform in all crystallographic directions, where all the properties of the materials are independent of the direction being measured [30]. β cosθ was plotted with respect to 4 sinθ for ZnO nanostructures peaks. Therefore the strain and crystallite size are calculated from the slope and y-intercept of the fitted line respectively (Fig. 4). The geometric parameters of ZnO nanostructures before and after annealing have been included in Table 2, which obtained from Scherrer's formula and W-H analysis.

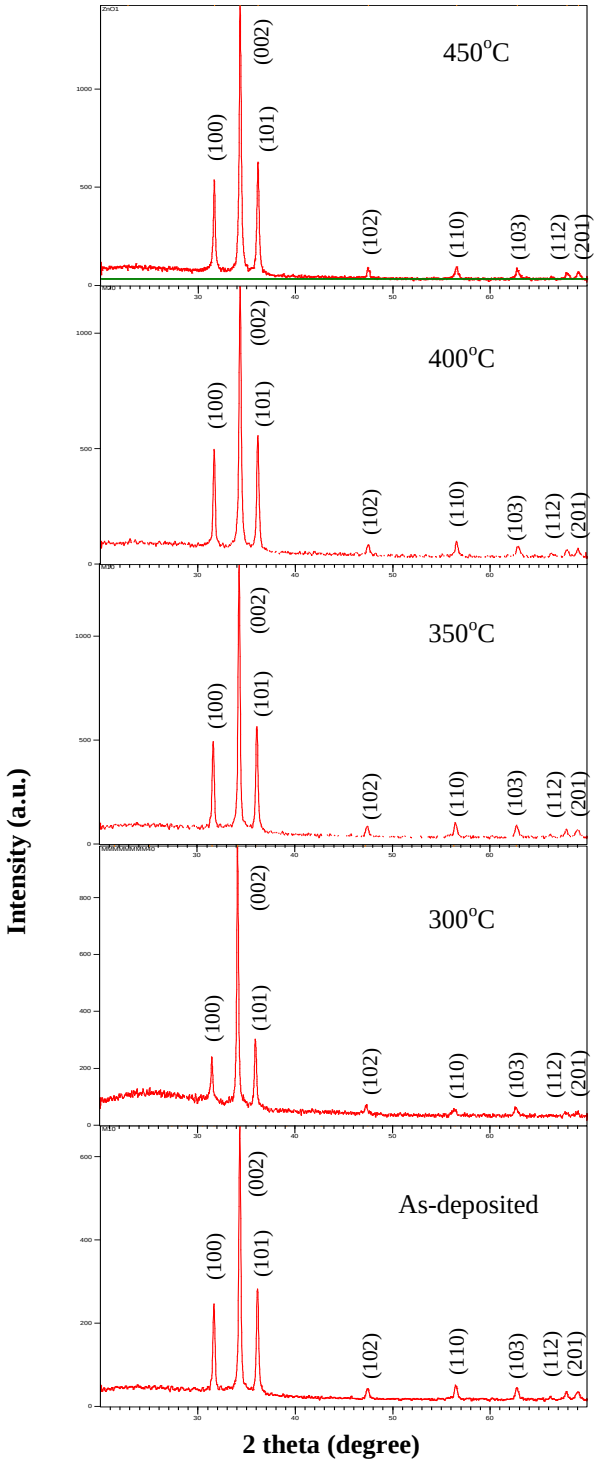

Figure 1: XRD pattern of ZnO nanostructures as-deposited and annealed at different temperatures.

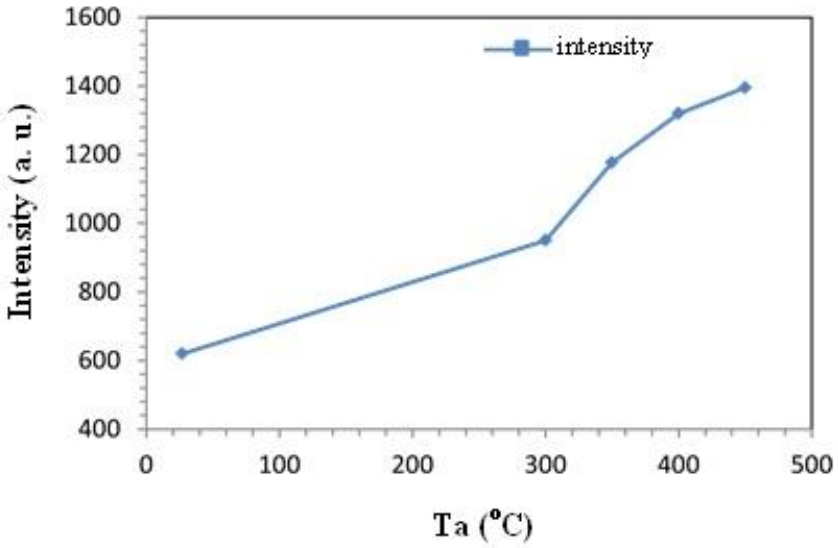

Figure 2: Effect of annealing temperature on XRD intensity.

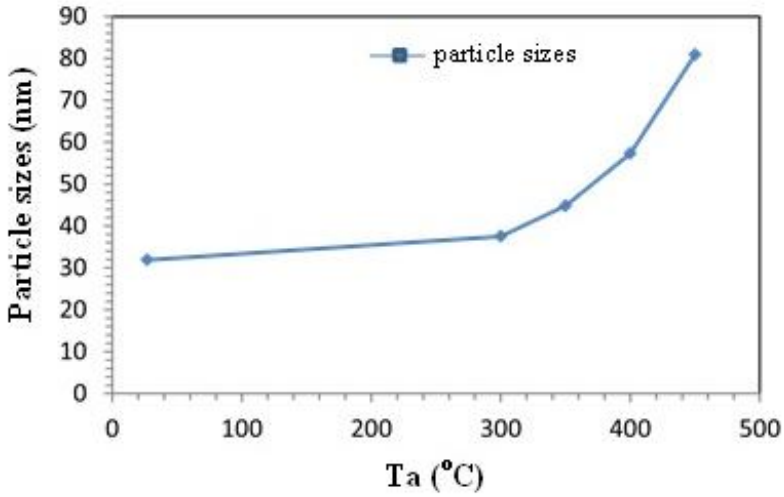

Figure 3: Effect of annealing temperature on particle size.

Table 1: Effect of Ta on structure parameters of ZnO nanostructures.

Ta (^oC)	2θ(^{o})	(hkl)	d_{XRD}(Å)	d_{JCPDS}(Å)	Lattice parameters (Å)	c/a	V (Å^3)
As-deposited (Hexagonal)	31.4817	(100)	2.8417	2.816	a=3.2786 c=5.2518	1.6018	48.89
	34.1221	(002)	2.6276	2.602			
	35.9481	(101)	2.4982	2.476			
	47.3054	(102)	1.9216	1.913			
	56.3098	(110)	1.6338	1.626			
	62.6567	(103)	1.4815	1.478			
	67.8668	(112)	1.3810	1.379			
	69.0077	(201)	1.3597	1.360			
300°C (Hexagonal)	31.4893	(100)	2.8411	2.816	a=3.2779 c=5.2510	1.6019	48.86
	34.1166	(002)	2.6281	2.602			
	35.9613	(101)	2.4974	2.476			
	47.2248	(102)	1.9247	1.913			
	56.3134	(110)	1.6337	1.626			
	62.6883	(103)	1.4808	1.478			
	67.8456	(112)	1.3814	1.379			
	69.0082	(201)	1.3609	1.360			
350°C (Hexagonal)	31.6424	(100)	2.8277	2.816	a=3.2624 c=5.2248	1.6015	48.16
	34.2980	(002)	2.6146	2.602			
	36.1162	(101)	2.4870	2.476			
	47.4414	(102)	1.9164	1.913			
	56.4466	(110)	1.6302	1.626			
	62.7515	(103)	1.4807	1.478			
	67.8148	(112)	1.3819	1.379			
	69.0077	(201)	1.3598	1.360			
400°C (Hexagonal)	31.6684	(100)	2.8254	2.816	a=3.2598 c=5.223	1.6022	48.06
	34.3259	(002)	2.6125	2.602			
	36.1482	(101)	2.4849	2.476			
	47.4762	(102)	1.9151	1.913			
	56.5646	(110)	1.6270	1.626			
	62.8369	(103)	1.4789	1.478			
	67.9000	(112)	1.3793	1.379			
	69.0519	(201)	1.3602	1.360			
450°C (Hexagonal)	31.6702	(100)	2.8253	2.816	a=3.2596 c=5.2207	1.6016	48.04
	34.3102	(002)	2.6115	2.602			
	36.1456	(101)	2.4850	2.476			
	47.4936	(102)	1.9144	1.913			
	56.5697	(110)	1.6269	1.626			
	62.8026	(103)	1.4796	1.478			
	67.9036	(112)	1.3803	1.379			
	69.0623	(201)	1.3589	1.360			

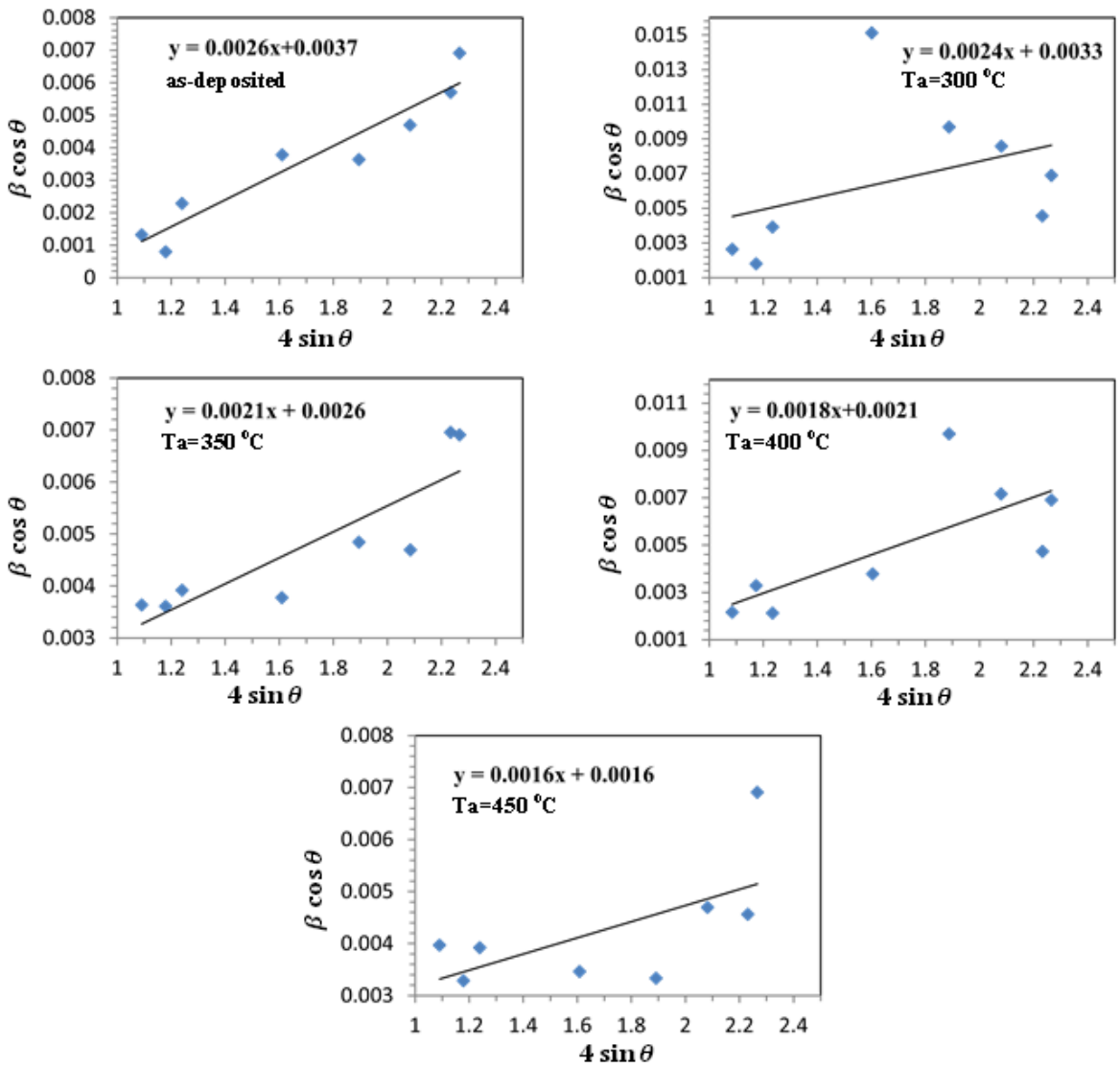

Figure 4: The W-H analysis of ZnO nanostructures before and after annealing assuming UDM.

Table 2: The values of some structural parameters of the studied ZnO nanostructures.

Ta (°C)	c/a	L (Å)	Scherer method		W-H method UDM	
			D (nm)	δ (x10^{14}) (Lines/m^2)	D (nm)	ε x10^{-3}
As-deposited	1.6018	1.9952	31.89	9.826	36.47	2.6
300°C	1.6019	1.9948	37.51	7.107	42.01	2.4
350°C	1.6015	1.9852	44.84	4.973	53.32	2.1
400°C	1.6022	1.9840	57.32	3.043	64.97	1.8
450°C	1.6016	1.9835	80.88	1.528	86.65	1.6

3.3. Surface and chemical composition characterization

Surface morphology of ZnO thin films was studied using scanning electron microscopy (SEM). Figure 5 (a)-(e) shows the SEM micrographs of the as-deposited and annealed at 300°C, 350°C, 400°C and 450°C of ZnO thin films. From the observation of the Figure we find that the surface morphology is formed from the growth of nanostructures with NNs randomly orientated with the preferred vertical orientation. As the Ta increases, it is notice that NNs become tapered to a sharper end at the top. When Ta increasing, the surface morphology of the thin films change and the grain size increases. That is, SEM results corroborated the results of XRD, where the size of the crystallite increases with increasing Ta. The difference in the value of grain size in the SEM study with the XRD analyses has been revealed due to different orientations [31], where the crystal size estimated by the XRD analyses was based on the highest diffraction intensity in a given plane direction. NNs are very important in electronic applications such as laser diodes, solar cells, gas sensors, field emitters and wave guides [32,33]. When the temperature rises to 450°C we get a structure shapes with regular triple branches. This regular branching consists initially of NNs containing effective zones for the compact growth of NNs in preferred growth directions (100), (002) and (101) forming a triple-homogeneous structure as shown in Fig. 5(e) (branching structures). Figure 6 shows EDS spectrum measurements of the ZnO nanostructures (for as-deposited). The atomic ratio of Zn to O was determined by the EDS measurement associated with SEM. From Fig. 6, we find that there are no impurities from other materials. The carbon peak can be attributed to either as a result of the heat from the deposition process due to the proximity of the films deposited from the zinc evaporation source or from the sample handling. The weight percentage of Zn and O elements is nearly stoichiometric (49.21 and 47.46, respectively), so the atomic ratio of Zn to O is 1.04.

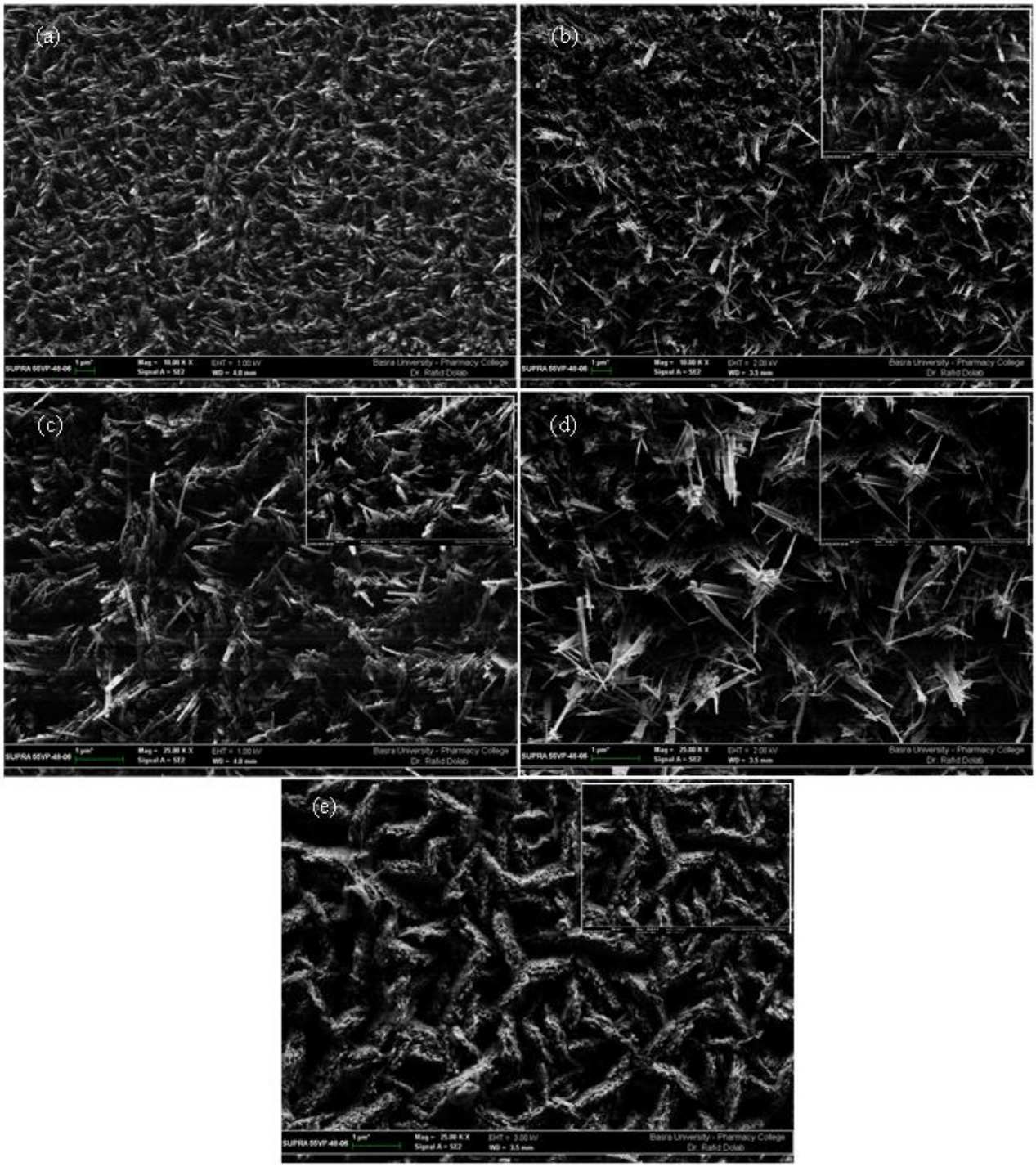

Figure 5: SEM surface micrographs of ZnO nanostructures and nano-branches before and after annealing at different temperatures: (a) as-deposited (b) 300°C (c) 350°C (d) 400°C and (e) 450°C (nano-branches). Inset of (b), (c), (d) and (e) shows the SEM images in the range of 200nm.

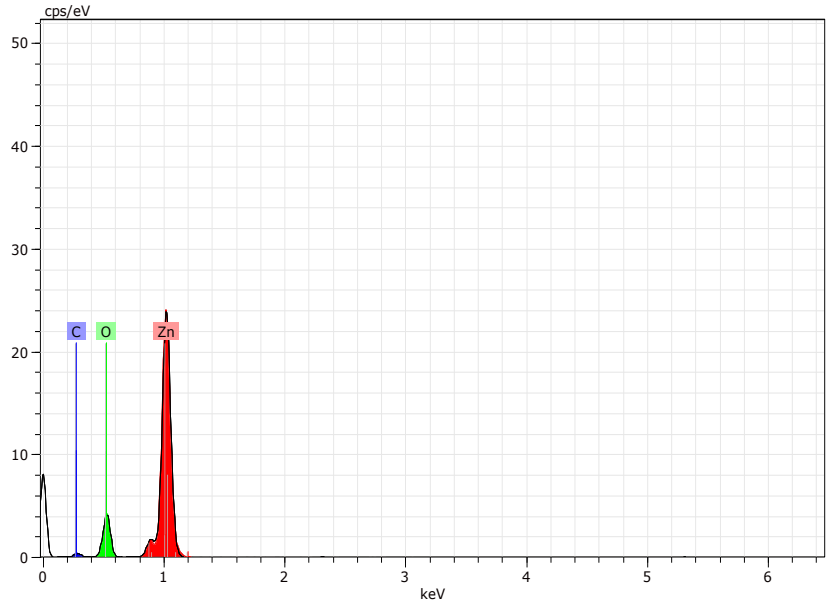

Figure 6: Chemical compositions of ZnO nanostructures.

3.4. Optical properties

Figures 7 and 8 represent the absorbance and transmittance spectra, respectively, for ZnO nanostructures thin films deposited and annealed at different temperatures. The possibility of obtaining high transmittance for the solar spectrum using ZnO thin films [34]. It can be observed from Fig. 8 that transmittance spectra present a sharp edge at a wavelength corresponding to the forbidden energy gap of ZnO thin films. This behavior shows that the studied films have a stoichiometric and homogeneous structure [35,36]. Figure 8 shows that all thin films are highly transparent, and the transmittance of these thin films increasing slightly with Ta. Surface morphology affects the optical transmittance of the film [37]. The average transmission values in the visible region were increased from 90% to 95% and it seems depending on the Ta. It is well known that investigation of the fundamental absorption edge of the semiconducting thin films provides important information on the characteristics of inter-band electronic transitions and the value of optical energy band gap [38,39]. The absorption peaks of ZnO nanostructures are strong in the range of ~ 360 nm to 380 nm, due to the transition of electrons from the valence band to the conduction band. From Fig. 7, there is a slight decrease in the absorption of samples with increasing Ta and the absorption edge slightly shift lower energy. The change in the band gap as a function of Ta may be causing the red shift of the absorption peak, which is in good agreement with that reported by other authors [40-42].

The optical absorption coefficient α was calculated for ZnO nanostructures thin films using the expression (15) [43,44]:

$$\alpha = 2.303\left(\frac{A}{t}\right) \quad (15)$$

Where, A is absorbance and t is the thickness.

It is well known that ZnO is a direct-gap semiconductor. The absorption coefficient α is related to the incident photon energy hυ as [45]:

$$(\alpha h\upsilon) = A\left(h\upsilon - E_g\right)^{1/2} \quad (16)$$

Where, A is a constant, Eg is the band gap, hν is the incident photon energy. The $(\alpha h\upsilon)^2$ vs. hυ plots for the ZnO nanostructures thin films, deposited and annealed samples were shown in Fig. 9. When the straight portion of $(\alpha h\upsilon)^2$ is extrapolated to the point of intercept in the X-axis (photon energy) gives the optical band gap (E_g) [46,47]. The values of optical band gaps for ZnO nanostructures thin films, as-deposited and annealed at different temperatures are 3.26eV, 3.20eV, 3.17eV, 3.10eV and 3.06eV, respectively. Which are in good agreement with the reported values by [41,42]. The decrease in band gap of thin films after annealing can be attributed to the increase in crystal size, which is consistent with crystallinity improvement deduced from XRD results. The high band gap value of ZnO thin films may be useful as buffer or/and window layers in thin film solar cells.

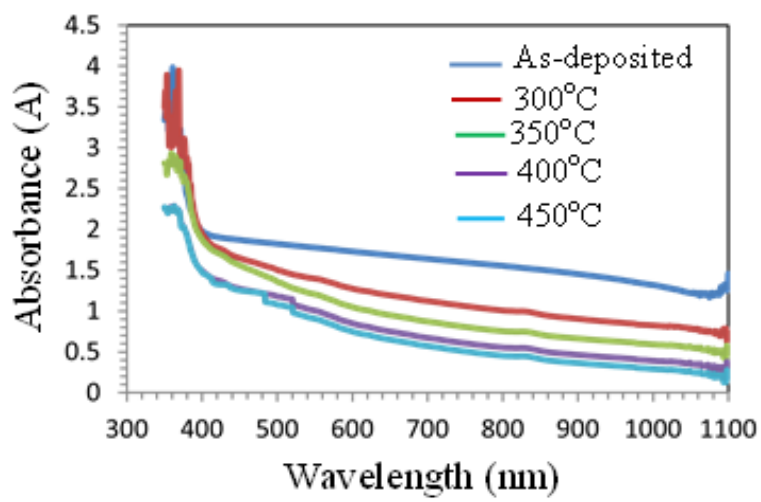

Figure 7: Absorbance spectra of ZnO nanostructures (as-deposited and annealed).

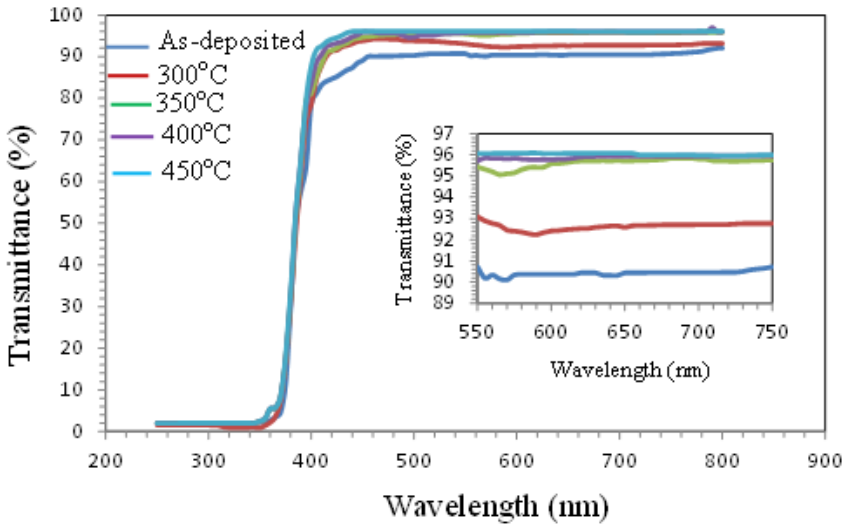

Figure 8: Optical transmittance spectra of ZnO nanostructures (as-deposited and annealed). Inset shows the transmission values in the visible region**.**

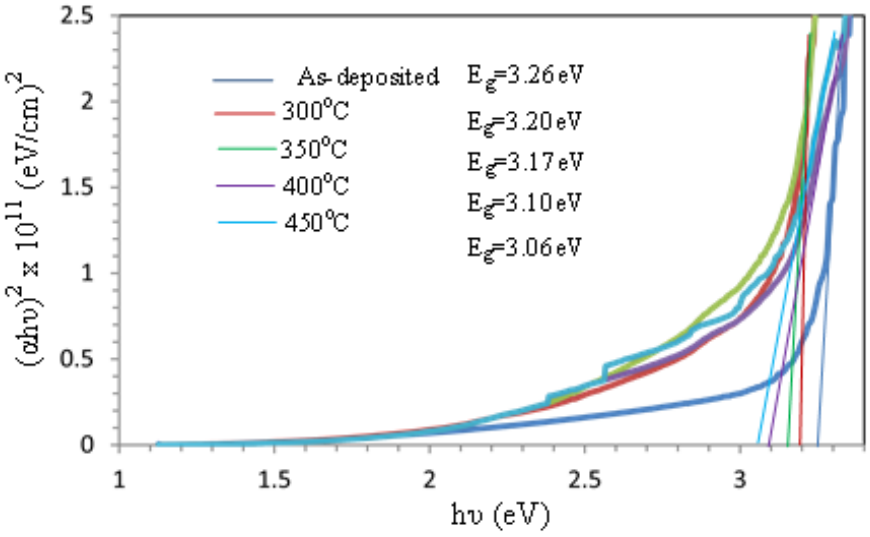

Figure 9: Plot of $(\alpha h\upsilon)^2$ versus hυ for ZnO nanostructures (as-deposited and annealed).

4. Conclusions

Thin films of ZnO nanostructures were successfully deposited on glass substrates at room temperature by thermal evaporation technique. Thin films were subjected to the annealing process at temperatures of 300 to 450°C for an hour. The effect of Ta on the structural,

morphological and optical properties of thin films of ZnO nanostructures was studied. XRD results showed that the ZnO nanostructures have hexagonal wurtzite phase, highly oriented with a c-axis plane (002) perpendicular to the substrate surface without any impurities. The high intensity of XRD is observed with increasing Ta which indicates crystalline improvement. The structural characteristics (lattice constant, crystallite size, dislocation density, bond length of Zn-O , strain, chemical composition, etc.) of the films studied by XRD, SEM and EDS show a good crystallinity columnar growth and smooth surface. The line broadening of ZnO nanostructures due to the small crystallite size and lattice strain was analyzed by Scherrer's formula and the method of W-H using UDM. From UV-Vis spectroscopy data, the typical exciton absorption was found at 363 nm and 368 nm, 372 nm, 377 nm and 380 nm is observed in the absorption spectrum corresponds to ZnO nanostructures before and after annealing, respectively. All the films exhibit high transmittance (90%-95%) in the visible region, thus making the films suitable for optoelectronic devices, for instance as window layers in solar cells. The values of the optical band gap energy decreased from 3.26 eV to 3.06 eV with increase the Ta.

References

[1] A. Facchetti and T. Marks; Transparent Electronics: From Synthesis To Applications, In: A. Facchetti, T. Marks, editors, Preface. Chichester, UK: Wiley; (2010).

[2] K. Ellmer, Past achievements and future challenges in the development of optically transparent electrodes, Nat Photon, (2012) 6809-17.

[3] J. Y. Noh, H. Kim, Y. S. Kim and CH. Park, Electron doping limit in Al-doped ZnO by donor-acceptor interactions, J. Appl. Phys. 113 (2013) 153703.

[4] YC. Lin, YC. Jian and JH. Jiang, A study on the wet etching behavior of AZO (ZnO:Al) transparent conducting film, Appl. Surf. Sci. 254 (2008) 2671-7.

[5] S. Das and S. Chaudhuri, Mg^{2+} substitutions in ZnO-Al_2O_3 thin films and its effect on the optical absorption spectra of the nanocomposite, Appl. Surf. Sci. 253, 21(2007) 8661-8668, ISSN: 0169-4332.

[6] Y. R. Ryu, S. Zhu, J. D. Budai, H. R. Chandrasekhar, P. F. Miceli and H. W. White, Optical and structural properties of ZnO films deposited on GaAs by pulsed laser deposition, J. Appl. Phys. 88, 1(2000) 201-204, ISSN: 0021-4922.

[7] L. Wang and N. C. Giles, Temperature dependence of the free-exciton transition energy in zinc oxide by photoluminescence excitation spectroscopy, J. Appl. Phys. 94, 2 (2003) 973-978, ISSN: 0021-4922.

[8] E. Pyne, G. P. Sahoo, K. Bhui, H. Bar, P. Sarkar, S. Samantsa, A. Maity and A. Misra, Enhanced photocatalytic activity of metal coated ZnO nanowires, Spectrochim. Acta. Part A, 93 (2012) 100-105.

[9] P. Wagner and R. Helbig, Halleffekt und anisotropie der beweglichkeit der elektronen in ZnO, J. Phys. Chem. Solids, 35 (1974) 327.

[10] T. Y. Kim, J. Y. Kim, S. H. Lee, H. W. Shim, E. K. Suh and K. S. Nahm, Characterization of ZnO needle-shaped nanostructures grown on NiO catalyst-coated Si substrates, Synth. Met. 144 (2004) 61-68.

[11] P. K. Baviskar, P. R. Nikam, S. S. Gargote, A. Ennaoui and B. R. Sankapal, Controlled synthesis of ZnO nanostructures with assorted morphologies via simple solution chemistry, J. Alloys Compd. 551 (2013) 233-242.

[12] Y. N. Xia, P. D. Yang, Y. G. Sun, Y. Y. Wu, B. Mayers, B. Gates, Y. D. Yin, F. Kim and H. Q. Yan, One-dimensional nanostructures: synthesis, characterization, and applications, Adv. Mater. 15 (2003) 353.

[13] J. J. Dong, C. H. Zhen, H. Y. Hao, J. Xing, Z. L. Zhang and Z. Y. Zheng, Controllable synthesis of ZnO nanostructures on the Si substrate by a hydrothermal route, J. Nano Letters, 8 (2013) 378.

[14] X. C. Chen, J. P. Zhou, H. Y. Wang, P.S. Xu and G. Q. Pan, " *In situ high temperature X-ray diffraction studies of ZnO thin film* " Chines Phys. B, 20 (2011) 096102, 1-3.

[15] S. Yilmaz, Study of influence of annealing time on some physical properties of ZnO:Cu nanorods grown by a simple chemical bath deposition method, J. Supercond. Nov. Magn., 27 (2014) 1083-1089.

[16] T. T. Miao, D. X. Sun, Y. R. Guo, C. Li, Y. L. Ma, G. Z. Fang and Q. J. Pan, Low-temperature precipitation synthesis of flower-like ZnO with lignin amine and its optical properties, J. Nano Letters, 8 (2013) 431.

[17] S. K. Chong, C. F. Dee and S. A. Rahman, Structural and photoluminescence studies on catalytic growth of silicon/zinc oxide heterostructure nanowires, J. Nano Letters, 8 (2013) 174.

[18] M. M. Ali, Characterization of ZnO thin films grown by chemical bath deposition, J. Basrah Researches (Sciences) 37 (3A) (2011) 49-55.

[19] X. D. Gao, X. M. Li and W. D. Yu, Rapid preparation, characterization, and photoluminescence of ZnO films by a novel chemical method, Mat. Res. Bulletin 40 (2005) 1104.

[20] B. D. Cullity and S. R. Stock, Elements of X-ray diffraction, 3rd edn. Prentice Hall, New Jersey (2001).

[21] A. B. Usseinov, E. A. Kotomin, A. T. Zhukovskii and J. Puans, Hydrogen induced metallization of ZnO (1100) surface: Ab initio study, Thin Solid Films 553 (2014) 38-42.

[22] J. Chang, A. Z. Muhammad, W. Wlodarski and E. R. Waclamik, Self-Assembled 3D ZnO Porous Structures with Exposed Reactive {0001} Facets and Their Enhanced Gas Sensitivity, Sensors, 13 (2013) 8445-8460.

[23] M. Saleem, L. Fang, H. B. Ruan, F. Wu, Q. L. Huang, C. L. Xu and C. Y. Kong, Effect of zinc acetate concentration on the structural and optical properties of ZnO thin films deposited by sol-gel method, Intl. J. Phys. Sci. 7 (23) (2012) 2971-2979.

[24] C. S. Barret and T. B. Massalski: Structure of Metals, Pergamon Press, Oxford (1980).

[25] Polycrystalline Semiconductors: Physical Properties and Applications, Ed. G. Harbeke, Springer-Verlag, Berlin (1985).

[26] S. J. Pearton, D. P. Norton, K. Ip, Y.W. Heo and T. Steiner, Recent progress in processing and properties of ZnO, J. Vac. Sci. Technol. B 22, 932 (2004).

[27] P. Bindu and S. Thomas, Estimation of lattice strain in ZnO nanoparticles: X-ray peak profile analysis, J. Theor. Appl. Phys. 8 (2014) 123-134.

[28] M. Soosen Samuel, L. Bose and KC. George, Optical properties of ZnO Nanoparticles, ISSN: 0973-7464, 16 (2009) 57-65.

[29] G. K. Williamson and W. H. Hall, " X-ray line broadening from filed aluminium and wolfram " Acta. Metall. 1 (1953) 22-31.

[30] V. Sesha Sai Kumar and K. Venkateswara Rao, X-ray Peak Broadening Analysis and Optical Studies of ZnO Nanoparticles Derived by Surfactant Assisted Combustion Synthesis , J. Nano-electron. phys. 5, 2, 02026 (2013) (6pp).

[31] M. Fakhar-E-Alam, M. A. Asghar, U. Nazar, S. Javed, Z. Iqbal and M. Atif, Characterization of zinc oxide (ZnO) thin film coated by thermal evaporation technique, J. Optoelectronics and Bio. Mate., 6, Issue 2 (2014) p. 35-40.

[32] Z. Han, L. Lia, Y. Wu, H. Pan, S. Shen and J. Chen, Synthesis and photocatalytic application of oriented hierarchical ZnO flower-rod architectures, J. Hazard. Mater, 217-218 (2012) 100-106.

[33] K. Kara, E. S. E. Tuzemen and R. Esen, Annealing effects of ZnO thin films on p-Si(100) substrate deposited, Turk J. Phys. 38 (2014) 238-244.

[34] S. Flickyngerova, A. Rehakova, V. Tvarozek and I. Novotny, Sputtered of ZnO:Al thin films for application in photovoltaic solar cell, Advances in Electrical and Electronic Engineering (2011) p. 382-84.

[35] E. K. Kim and Y.S. Kim, The effect on the annealing temperature of Li doped ZnO thin film for a film bulk acoustic resonator, Superlattices and Microstruct. 42 (2007) 343-347.

[36] J. Benn, P. R. Manyon and V. K. Vaedyan, Studies on preparation and characterization of indium doped zinc oxide films by chemical spray deposition, Bull. Mater. Sci. 28(5) (2005) 487.

[37] T. Prasada Rao and M. C. Santhosh Kumar, Realization of stable p-type ZnO thin films using Li-N dual acceptors, J. Alloys and Compounds 509 (2011) 8676-8682.

[38] K. L. Chopra, Thin Film Phenomena, McGraw-Hill, New York 1969.

[39] J. N. Pankove, Optical Processes in Semiconductors, Dover, New York 1971.

[40] T. D. Malevu and R. O. Ocaya, Effect of annealing temperature on structural, morphology and optical properties of ZnO nano-needles prepared by Zinc-Air cell system method, Int. J. Electrochem. Sci. 10 (2015) 1752-1761.

[41] S. Sanjeev and D. Kekuda, Effect of annealing temperature on the structural and optical properties of zinc oxide (ZnO) thin films prepared by spin coating process, IOP Conf. Series: Materials Science and Engineering **73** (2015) 012149 (5pp).

[42] J. Husna, M. Mannir Aliyu, M. Aminul Islam, P. Chelvanathan, N. Radhwa Hamzah, M. Sharafat Hossain, M. R. Karim and N. Amin, Influence of annealing temperature on the properties of ZnO thin films grown by sputtering, Energy Procedia 25 (2012) 55-61.

[43] M. M. Ali, S. J. Abbas and A. S. Al-Kabbi, Effect of Annealing Temperature on Structural and Optical Properties of CdS Thin Films Prepared by CBD and Thermal Evaporation Techniques, J. Basrah Researches ((Sciences)), Vol. (45), No. 1 (2019), 1-12.

[44] Kumar 1, K. Balachandraand and P. Raji, Synthesis and characterization of nano zinc oxide by sol-gel spin coating, Recent Research in Science and Technology 3(3) (2011) 48-52.

[45] J. Tauc, The Optical Properties of Solids, North-Holland, Amsterdam (1970).

[46] F. Chaabouni, M. Abaab and B. Rezig, Effect of the substrate temperature on the properties of ZnO films grown by RF magnetron sputtering, Mater. Sci. and Eng. B109, (2004) 236-40.

[47] M. M. Ali, *" Annealing Temperature Dependent Structural, Optical and Electrical Properties of Thermally Deposited CdSe Thin Films " Journal of Basrah Researches ((Sciences)) Vol. (44). No. 1 (2018), 33-45.*

تأثير درجة حرارة التلدين على خواص التراكيب النانوية لـ *ZnO*

محمــد محسـن علي و سعيد جبار عباس و علاء شاوي الكعبي

قسم الفيزياء، كلية العلوم، جامعة البصرة، البصرة، العراق

المستخلص

تمت دراسة تأثير عملية التلدين على خواص التراكيب النانوية والتي تحتوي على الابر النانوية لـ ZnO باستخدام تقنيات *XRD* و *SEM* و مطياف UV-visible في مدى درجات الحرارة من 300 الى $450^{O}C$. أوضحت قياسات XRD ان التراكيب النانوية أو الابر النانوية لـ ZnO المودعة والملدنة كانت بدون شوائب خارجية (غريبة) مع تركيب سداسي wurtzite. المستوي (002) هو المستوي المفضل للأغشية الرقيقة للتراكيب النانوية وللآبر النانوية لـ ZnO. تم تحديد معلمات الشبيكة، الحجم البلوري، طول الحزمة بين Zn و O (Zn-O) للأغشية الرقيقة لـ ZnO nanostructures. كانت قيم ثوابت الشبيكة a=b=3.278 Å و c=5.251 Å للأغشية المودعة ولوحظ انها تتناقص تدريجيا الى a=b=3.259 Å و c=5.220 Å بعد التلدين عند درجة حرارة $450^{O}C$. الزيادة في درجة حرارة التلدين تؤدي الى الزيادة في شدة قمم الحيود. عند زيادة درجة حرارة التلدين فان حجم الجسيم يزداد وكذلك طول الابر النانوية تزداد وتصبح اكثر اتجاهية. تم استخدام تحليل W-H لحساب احجام البلورات والاجهاد الشبيكي بالاعتماد على تحليلات اتساع قمة الاشعة السينية. تبين النتائج ان هناك ارتباط وثيق عالي بين تقديرات حجم الجسيم الناتج من تحليلات SEM وحجم الجسيم الناتج من علاقة شيرار ومخططات W-H. تبين القياسات الضوئية ان الاغشية كانت شفافة ضوئيا للمنطقة المرئية من طيف الاشعة الكهرومغناطيسية مع معدل نفاذية من 90% الى 95% والتي تكون معتمدة على درجة حرارة التلدين. لاحظنا وجود بعض الاتفاق بين قيمة فجوة الحزمة المقدرة من القياسات الضوئية مع قيمة فجوة الحزمة لـ ZnO في الحالة الصلبة (بالنسبة للأغشية المودعة من ZnO nanostructures). أن فجوة الطاقة تقل مع درجة حرارة التلدين، E_g=3.26 eV بالنسبة للأغشية المودعة وبعد التلدين تقل الى 3.20 eV و 3.17 eV و 3.10 eV و 3.06 eV، على التوالي.